

Advantages of Asynchronous Measurement-Device-Independent Quantum Key Distribution in Intercity Networks

Yuan-Mei Xie,¹ Jun-Lin Bai,¹ Yu-Shuo Lu,¹ Chen-Xun Weng,¹ Hua-Lei Yin,^{1,*} and Zeng-Bing Chen^{1,†}

¹*National Laboratory of Solid State Microstructures and School of Physics,
Collaborative Innovation Center of Advanced Microstructures, Nanjing University, Nanjing 210093, China*

The new variant of measurement-device-independent quantum key distribution (MDI-QKD), asynchronous MDI-QKD, offers similar repeater-like rate-loss scaling but has the advantage of simple technology implementation by exploiting an innovative post-measurement pairing technique. We herein present an evaluation of the practical aspects of decoy-state asynchronous MDI-QKD. To determine its effectiveness, we analyze the optimal method of decoy-state calculation and examine the impact of asymmetrical channels and multi-user networks. Our simulations show that, under realistic conditions, asynchronous MDI-QKD can furnish the highest key rate with MDI security as compared to other QKD protocols over distances ranging from 50 km to 480 km. At fiber distances of 50 km and 100 km, the key rates attain 6.02 Mbps and 2.29 Mbps respectively, which are sufficient to facilitate real-time one-time-pad video encryption. Our findings indicate that experimental implementation of asynchronous MDI-QKD in intercity networks can be both practical and efficient.

I. INTRODUCTION

Quantum key distribution (QKD) [1, 2] enables remote two parties to share secret keys protected from eavesdropping by the laws of physics. In the past forty years, QKD has achieved rapid development in terms of secret key rates [3–6], transmission distance [7–9] and network deployment [10–13]. Although the security of QKD has been proven in theory, the imperfections of realistic devices lead to various security loopholes [14–16], especially in detection [15].

Fortunately, measurement-device-independent (MDI) QKD is proposed [17], which assumes an untrusted intermediate node to perform two-photon Bell state measurements, thus solving all security issues at the detection side [18]. Extensive work demonstrates the potential of MDI-QKD, including experimental breakthroughs [19–25], on-chip implementations [26–28], and continuous theoretical developments [29–34]. Moreover, users in a MDI-QKD network can share expensive detectors, and the topology of MDI-QKD is naturally suitable for deployment in star-type networks. Additionally, side-channel-secure QKD has recently been experimentally realized, which is not only MDI but also immune to potential source imperfections [35, 36]. However, the key rates of most forms of QKD are fundamentally bounded by the secret key capacity of repeaterless QKD [37–40] due to photon loss in the channel. A rigorous theorem, the absolute repeaterless secret key capacity (SKC_0), expresses this limit as $R = -\log_2(1 - \eta)$ [39], i.e., the key rate R scales linearly with the channel transmittance η . Despite some progress in overcoming this bound [41–44], such devices remain elusive.

Twin-field (TF) QKD [45] and its variants [46–51] are proposed to break this bound. The protocols make

the untrusted intermediate node use Bell state measurements based on single-photon interference, rather than two-photon interference. Numerous works have advanced theory with finite key analysis [52–55]. Ref. [56] applies entangled coherent state sources as untrusted relays to further increase the transmission distance of TF-QKD by reducing the signal-to-noise ratio at the measurement nodes. Several experimental achievements have shown the performance of twin-field QKD over large loss [57–70], and the maximum distance of TF-QKD has been experimentally increased to 830 kilometers [68]. The idea of single-photon interference has also been implemented in device independent QKD [71]. Nonetheless, as TF-QKD requires stable long-distance single-photon interference, phase-tracking and phase-locking techniques are indispensable [45]. These techniques are complicated and expensive, and usually impose a negative impact on the system performance. For example, phase tracking technology requires sending strong reference light, which reduces the effective clock frequency of the quantum signal and increases background noise [61, 62, 67, 68].

Recently, the new variant [72, 73] of MDI-QKD, called asynchronous MDI-QKD [72] (also called mode-pairing MDI-QKD [73]), is proposed. It asynchronously pairs two successful clicks within a long pairing time to establish two-photon Bell state, thereby breaking SKC_0 . Asynchronous MDI-QKD is highly practical and has a noteworthy advantage over TF-QKD in intercity-distance quantum communications, owing to its implementation simplicity and performance. Several exciting experiments have successfully verified the superior performance of asynchronous MDI-QKD with accessible technology. Ref. [74] realizes the experiment with a maximal distance of 407 km without global phase locking. Ref. [75] demonstrates the first asynchronous MDI-QKD that overcomes SKC_0 without global phase tracking and extends the maximal distance to 508 km. However, before asynchronous MDI-QKD can be applied in real life, many issues of practicality necessitate resolution, such

* hlyin@nju.edu.cn

† zbchen@nju.edu.cn

as identifying the optimal number of decoy states, determining the optimal calculation method of decoy states, and assessing the performance in asymmetric channels and networks.

In this work, we address these issues by introducing the joint-constraints technique [76] and new methods for phase error rate estimation to enable higher-rate asynchronous MDI-QKD. By employing the three-intensity protocol alongside an additional *click filtering* operation—which is the known best choice for performance—we simulate the key rate of asynchronous MDI-QKD in multi-user networks. For a network of five users, asynchronous MDI-QKD result in the key rates of all links surpassing the secret key capacity. Furthermore, using a 4 GHz repetition rate system [68], secret key rates of 6.02 Mbps, 2.29 Mbps, and 0.31 Mbps can be achieved at fiber distances of 50 km, 100 km, and 200 km, respectively. Asynchronous MDI-QKD can achieve the highest key rate in the range of 170 to 480 km, compared with decoy-state QKD [77–79] and TF-QKD [45]. More importantly, our work provides conceptual differences between asynchronous MDI-QKD and its synchronous version (original time-bin MDI-QKD) [80]. Asynchronous MDI-QKD holds the most promising potential as a solution for short-distance quantum communication in the future, owing to its minimal detector requirements and absence of strong light feedback.

II. PROTOCOL DESCRIPTION

Here, we consider an asymmetric asynchronous MDI-QKD protocol using three-intensity settings. The intensity of each laser pulse is randomly set to one of the three intensities $\mu_{a(b)}$ (signal), $\nu_{a(b)}$ (decoy) and $o_{a(b)}$ (vacuum), and the intensities satisfy $\mu_{a(b)} > \nu_{a(b)} > o_{a(b)} = 0$. A successful click is obtained when one and only one detector clicks in a time bin, and we refer to $(k_a|k_b)$ as a successful click when Alice sends intensity k_a and Bob sends k_b . The notation $[k_a^{\text{tot}}, k_b^{\text{tot}}]$ indicates an asynchronous coincidence where the combined intensity in the two time-bins Alice (Bob) sent is k_a^{tot} (k_b^{tot}). The details of the protocol are presented as follows.

1. *Preparation.* For each time bin, Alice chooses a phase value $\theta_a = 2\pi M_a/M$ with $M_a \in \{0, 1, \dots, M-1\}$ at random. Then, she selects an intensity choice $k_a \in \{\mu_a, \nu_a, o_a\}$ with probabilities p_{μ_a} , p_{ν_a} , and $p_{o_a} = 1 - p_{\mu_a} - p_{\nu_a}$, respectively. Alice prepares a weak laser pulse $|e^{i\theta_a} \sqrt{k_a}\rangle$ based on the chosen values. Similarly, Bob prepares a weak coherent pulse $|e^{i\theta_b} \sqrt{k_b}\rangle$ ($k_b \in \{\mu_b, \nu_b, o_b\}$). Finally, Alice and Bob send their optical pulses to Charlie via the quantum channel.

2. *Measurement.* For each time bin, Charlie performs a first-order interference measurement on the two received pulses, and he publicly announces whether a successful click is obtained and which detector (D_L or D_R) clicked. The first two steps will be repeated N times.

3. *Coincidence pairing.* The clicks that Alice and Bob

retained for further processing depend on whether *click filtering* is applied. If they perform *click filtering*, Alice (Bob) announces whether she (he) applied the decoy intensity ν_a (ν_b) to the pulse sent for each event. Then they discard clicks $(\mu_a|\nu_b)$ and $(\nu_a|\mu_b)$, and keep all other clicks. Otherwise, they keep all clicks.

For all kept clicks, Alice and Bob always pair a click with the nearest one within a time interval T_c to form a successful coincidence. They discard the lone click that failed to find a partner within T_c . For each coincidence, Alice (Bob) computes the total intensity used between the two time bins k_a^{tot} (k_b^{tot}) and the phase differences between the early (e) and late (l) time bins, $\varphi_{a(b)} = \theta_{a(b)}^l - \theta_{a(b)}^e$.

4. *Sifting.* Alice and Bob announce their computational results and then discard the data if $k_a^{\text{tot}} \geq \mu_a + \nu_a$ or $k_b^{\text{tot}} \geq \mu_b + \nu_b$. When there is a *click filtering* operation, we define $\tilde{k}_{a(b)} = \mu_{a(b)}$; otherwise, we define $\tilde{k}_{a(b)} \in \{\mu_{a(b)}, \nu_{a(b)}\}$. For $[\tilde{k}_a, \tilde{k}_b]$ coincidence, Alice (Bob) extracts a \mathbf{Z} -basis bit 0 (1) if she (he) sends $\tilde{k}_{a(b)}$ in the early time bin and $o_{a(b)}$ in the late time bin. Otherwise, Alice (Bob) extracts an opposite bit. Note that we use four intensity groups ($[\mu_a, \mu_b]$, $[\mu_a, \nu_b]$, $[\nu_a, \nu_b]$, $[\nu_a, \mu_b]$) for the key generation when *click filtering* is not applied, while existing MDI-QKD protocols typically use only one intensity group. For $[2\nu_a, 2\nu_b]$ coincidence, Alice and Bob calculate the relative phase difference $\varphi_{ab} = (\varphi_a - \varphi_b) \bmod 2\pi$. They extract an \mathbf{X} -basis bit 0 if $\varphi_{ab} = 0$ or π . Afterwards, Bob flips his bit value, if $\varphi_{ab} = 0$ and both detectors clicked, or $\varphi_{ab} = \pi$ and the same detector clicked twice. The coincidence with other phase differences is discarded.

5. *Parameter estimation.* Alice and Bob group their data into different sets $\mathcal{S}_{[k_a^{\text{tot}}, k_b^{\text{tot}}]}$ and count the corresponding number $n_{[k_a^{\text{tot}}, k_b^{\text{tot}}]}$. By using all the raw data they have obtained, Alice and Bob estimate the necessary parameters to calculate the key rate. They estimate the number of vacuum events, s_0^z , the number of single-photon pair events in the \mathbf{Z} basis, s_{11}^z , the bit error rate of the single-photon pairs in the \mathbf{X} basis, e_{11}^x , and the phase error rate associated with the single-photon pair events in the \mathbf{Z} basis, ϕ_{11}^z .

6. *Key distillation.* Alice and Bob perform an error correction step that reveals at most λ_{EC} bits of information. Under the condition of passing the checks in the error correction and privacy amplification steps, a ε_{tot} -secret key of length

$$\ell = \underline{s}_0^z + \underline{s}_{11}^z \left[1 - H_2 \left(\bar{\phi}_{11}^z \right) \right] - \lambda_{\text{EC}} \quad (1)$$

$$\log_2 \frac{2}{\varepsilon_{\text{cor}}} - 2 \log_2 \frac{2}{\varepsilon' \hat{\varepsilon}} - 2 \log_2 \frac{1}{2\varepsilon_{\text{PA}}},$$

can be extracted, where \underline{x} and \bar{x} are the lower and upper bounds of the observed value x , respectively; $H_2(x) = -x \log_2 x - (1-x) \log_2 (1-x)$ is the binary Shannon entropy function. Using the entropic uncertainty relation [75], the total secure coefficient $\varepsilon_{\text{tot}} =$

$2(\varepsilon' + 2\varepsilon_e + \hat{\varepsilon}) + \varepsilon_0 + \varepsilon_1 + \varepsilon_\beta + \varepsilon_{\text{PA}} + \varepsilon_{\text{cor}}$, where ε_{cor} is the failure probability of error correction; ε_{PA} is the failure probability of privacy amplification; $\hat{\varepsilon}$ and ε' are the coefficients while using a chain-rule for smooth entropies; ε_0 , ε_1 and ε_β are the failure probabilities for estimating the terms of s_0^z , s_{11}^z , and e_{11}^x , respectively.

III. THE KEY RATE FORMULA

In the following description, let x^* be the expected value of x . In the asynchronous MDI-QKD protocol, $[\tilde{k}_a, \tilde{k}_b]$ coincidence can be used to generate keys. Since the binary Shannon entropy function is concave, we can correct errors for each group $[\tilde{k}_a, \tilde{k}_b]$ separately to reduce the consumption of information, which does not affect the security of the protocol. Hence the amount of information consumed in error correction can be written as

$$\lambda_{\text{EC}} = \sum_{\tilde{k}_a, \tilde{k}_b} \left[n_{[\tilde{k}_a, \tilde{k}_b]} f H_2 \left(E_{[\tilde{k}_a, \tilde{k}_b]} \right) \right], \quad (2)$$

where f is the error correction efficiency and $E_{[\tilde{k}_a, \tilde{k}_b]}$ is the bit error rate of $[\tilde{k}_a, \tilde{k}_b]$ coincidence. Because vacuum states contain no information about their bit values, in the asymmetric case we can separately extract higher-valued vacuum components in each group $[\tilde{k}_a, \tilde{k}_b]$ to obtain higher key rates. The total number of vacuum components in the \mathbf{Z} basis can be given by

$$s_0^{z*} = \sum_{\tilde{k}_a, \tilde{k}_b} \max \left\{ \frac{e^{-\tilde{k}_a} p_{[\tilde{k}_a, \tilde{k}_b]} n_{[o_a, \tilde{k}_b]}^*}{p_{[o_a, \tilde{k}_b]}}, \frac{e^{-\tilde{k}_b} p_{[\tilde{k}_a, \tilde{k}_b]} n_{[\tilde{k}_a, o_b]}^*}{p_{[\tilde{k}_a, o_b]}} \right\}. \quad (3)$$

Here $p_{[k_a^{\text{tot}}, k_b^{\text{tot}}]}$ is the probability that $[k_a^{\text{tot}}, k_b^{\text{tot}}]$ coincidence occurs given the coincidence event, which is

$$p_{[k_a^{\text{tot}}, k_b^{\text{tot}}]} = \sum_{k_a^e + k_a^l = k_a^{\text{tot}}} \sum_{k_b^e + k_b^l = k_b^{\text{tot}}} \frac{p_{k_a^e} p_{k_b^e}}{p_s} \frac{p_{k_a^l} p_{k_b^l}}{p_s}. \quad (4)$$

When *click filtering* is not applied, $p_s = 1$, otherwise $p_s = 1 - p_{\mu_a} p_{\nu_b} - p_{\nu_a} p_{\mu_b}$.

Next, we need to estimate the number and phase error rate of the single-photon pairs in the \mathbf{Z} basis, s_{11}^z and ϕ_{11}^z . Because the density matrices of single-photon pairs in the \mathbf{Z} basis are equal to those in the \mathbf{X} basis, the single-photon pair yields in the two bases are equal. For the same reason, we can estimate the single-photon pair phase error rate in the \mathbf{Z} basis according to the single photon-pair bit error rate in the \mathbf{X} basis. Therefore, in all single-photon pairs, the expected ratio of different intensity settings is the same as that of the emitted states,

$$\frac{s_{11}^{z*}}{s_{11}^{x*}} = \frac{t_{11}^{z*}}{t_{11}^{x*}} = \frac{\sum_{\tilde{k}_a, \tilde{k}_b} (\tilde{k}_a \tilde{k}_b e^{-\tilde{k}_a - \tilde{k}_b} p_{[\tilde{k}_a, \tilde{k}_b]})}{4\nu_a \nu_b e^{-2\nu_a - 2\nu_b} p_{[2\nu_a, 2\nu_b]}}. \quad (5)$$

Then we estimate the lower bound of s_{11}^{z*} using the decoy-state method [77–79], which can be given by

$$\begin{aligned} s_{11}^{z*} = & \frac{\sum_{\tilde{k}_a, \tilde{k}_b} (\tilde{k}_a \tilde{k}_b e^{-\tilde{k}_a - \tilde{k}_b} p_{[\tilde{k}_a, \tilde{k}_b]})}{\nu_a \nu_b \mu_a \mu_b (\mu' - \nu')} \\ & \times \left[\mu_a \mu_b \mu' \left(e^{\nu_a + \nu_b} \frac{n_{[\nu_a, \nu_b]}^*}{p_{[\nu_a, \nu_b]}} - e^{\nu_b} \frac{\bar{n}_{[o_a, \nu_b]}^*}{p_{[o_a, \nu_b]}} \right. \right. \\ & \left. \left. - e^{\nu_a} \frac{\bar{n}_{[\nu_a, o_b]}^*}{p_{[\nu_a, o_b]}} + \frac{n_{[o_a, o_b]}^*}{p_{[o_a, o_b]}} \right) \right. \\ & \left. - \nu_a \nu_b \nu' \left(e^{\mu_a + \mu_b} \frac{\bar{n}_{[\mu_a, \mu_b]}^*}{p_{[\mu_a, \mu_b]}} - e^{\mu_b} \frac{n_{[o_a, \mu_b]}^*}{p_{[o_a, \mu_b]}} \right. \right. \\ & \left. \left. - e^{\mu_a} \frac{n_{[\mu_a, o_b]}^*}{p_{[\mu_a, o_b]}} + \frac{n_{[o_a, o_b]}^*}{p_{[o_a, o_b]}} \right) \right], \end{aligned} \quad (6)$$

where

$$\begin{cases} \mu' = \mu_a, & \nu' = \nu_a, & \text{if } \frac{\mu_a}{\mu_b} \leq \frac{\nu_a}{\nu_b}, \\ \mu' = \mu_b, & \nu' = \nu_b, & \text{if } \frac{\mu_a}{\mu_b} > \frac{\nu_a}{\nu_b}. \end{cases} \quad (7)$$

We can use the technique of joint constraints [76] to obtain the tighter estimated value of s_{11}^{z*} . The details of the analytic results of joint constraints are shown in Appendix A. Then we can obtain the lower bound of s_{11}^{x*} with Eq. (5).

The upper bound of the single-photon pair errors of the \mathbf{X} basis is

$$\bar{t}_{11}^x = m_{[2\nu_a, 2\nu_b]} - \underline{m}_{[2\nu_a, 2\nu_b]}^0, \quad (8)$$

where $m_{[2\nu_a, 2\nu_b]}$ is the observed error bit number in the \mathbf{X} basis, and $\underline{m}_{[2\nu_a, 2\nu_b]}^0$ is the error bit number in the \mathbf{X} basis given that at least one of Alice and Bob sends vacuum component. The lower bound of the expected value $\underline{m}_{[2\nu_a, 2\nu_b]}^{0*}$ can be given by

$$\begin{aligned} \underline{m}_{[2\nu_a, 2\nu_b]}^{0*} = & \frac{e^{-2\nu_a} p_{[2\nu_a, 2\nu_b]} n_{[o_a, 2\nu_b]}^*}{2p_{[o_a, 2\nu_b]}} + \frac{e^{-2\nu_b} p_{[2\nu_a, 2\nu_b]} n_{[2\nu_a, o_b]}^*}{2p_{[2\nu_a, o_b]}} \\ & - \frac{e^{-2\nu_a - 2\nu_b} p_{[2\nu_a, 2\nu_b]} \bar{n}_{[o_a, o_b]}^*}{2p_{[o_a, o_b]}}. \end{aligned} \quad (9)$$

Similarly, we obtain the tighter value of $\underline{m}_{[2\nu_a, 2\nu_b]}^{0*}$ under the joint constraints [76]. According to the formula of

TABLE I. Simulation parameters. Here $\eta_d = \eta_d^L = \eta_d^R$, $p_d = p_d^L = p_d^R$, and η_d^L (η_d^R) and p_d^L (p_d^R) are the detection efficiency and the dark count rate of the detector D_L (D_R), respectively; α denotes the attenuation coefficient of the fiber; ω_{fb} is the fiber phase drift rate; E_{HOM} is the interference misalignment error rate; f is the error correction efficiency; $\Delta\nu$ is the laser frequency difference; and ϵ is the failure probability considered in the error verification and finite data analysis.

η_d	p_d	α	ω_{fb}	E_{HOM}	f	$\Delta\nu$	ϵ
80%	0.1 Hz	0.16 dB/km	5900 rad/s	0.04	1.1	10 Hz	10^{-10}

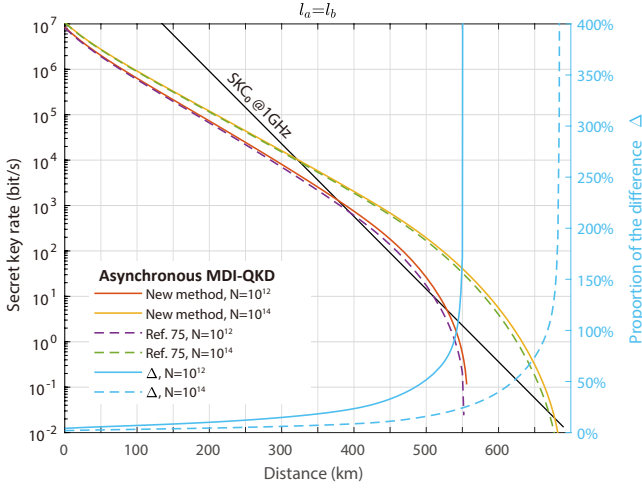


FIG. 1. Secret key rates of the three-intensity asynchronous MDIQKD protocol with *click filtering* using different phase error rate estimation methods. The numerical results here show that the new phase error rate estimation method has a notable advantage.

random sampling without replacement in Ref. [81], we can obtain the estimated value of the phase error rate of the single-photon pair events in the \mathbf{Z} basis

$$\bar{\phi}_{11}^z = \frac{\bar{t}_{11}^x}{\underline{s}_{11}^x} + \gamma \left(\underline{s}_{11}^z, \underline{s}_{11}^x, \frac{\bar{t}_{11}^x}{\underline{s}_{11}^x}, \varepsilon_e \right), \quad (10)$$

where

$$\gamma^U(n, k, \lambda, \epsilon) = \frac{\frac{(1-2\lambda)AG}{n+k} + \sqrt{\frac{A^2G^2}{(n+k)^2} + 4\lambda(1-\lambda)G}}{2 + 2\frac{A^2G}{(n+k)^2}}, \quad (11)$$

with $A = \max\{n, k\}$ and $G = \frac{n+k}{nk} \ln \frac{n+k}{2\pi nk\lambda(1-\lambda)\epsilon^2}$. From another viewpoint, we can calculate t_{11}^{x*} by

$$\bar{t}_{11}^{x*} = m_{[2\nu_a, 2\nu_b]}^* - \underline{m}_{[2\nu_a, 2\nu_b]}^{0*}, \quad (12)$$

and obtain \bar{t}_{11}^{z*} by Eq. (5). Then we calculate the observed values of \bar{t}_{11}^{z*} and \underline{s}_{11}^{z*} with the Chernoff bound (see Eqs. (E1) and (E2) in Appendix E). The upper bound of the single-photon pair phase error rate in the \mathbf{Z} basis can be written as

$$\bar{\phi}_{11}^z = \frac{\bar{t}_{11}^z}{\underline{s}_{11}^z}. \quad (13)$$

IV. PERFORMANCE

A. Optimal decoy-state method

For the evaluation, we numerically optimize the secret key rate $R := \ell F/N$ of asynchronous-MDIQKD

with Eq. (10) (original method [75]) and Eq. (13) (new method), which is shown in Fig. 1. Here F is the system clock frequency. In this work, we set failure parameters ε_{cor} , ε' , ε_e , $\hat{\varepsilon}$, ε_β , and ε_{PA} to be the same value: ϵ . The experimental parameters are set to the values used in the state-of-the-art system, as shown in Table I. In Fig. 1, we set $F = 1$ GHz and $l_a = l_b$, and the source parameters of Alice and Bob are all the same. The genetic algorithm is exploited to globally search for the optimal value of light intensities and their corresponding probabilities. The gray line is the results of SKC_0 . The results show that as the distance increases, the influence of statistical fluctuations becomes increasingly significant, and the key rate advantage of the new phase error rate estimation method is also increasing. For example, at a fiber length of 600 km with $N = 10^{14}$, the secret key rate obtained by the new phase error rate estimation method is approximately 1.49 times that of the original method. In the following key rate calculations, we use the new phase error rate estimation method by default.

B. Optimal protocol

Figure 2 shows a comparison of the secret key rates of asynchronous MDI-QKD with and without *click filtering* under symmetrical $l_a = l_b$ and asymmetrical channels $l_a - l_b = 100$ km. The parameters are listed in Table I. $F = 1$ GHz and $N = 10^{13}$ are used. The green dotted line is results of using only $[\mu_a, \mu_b]$ coincidence to form the secret key without *click filtering*. In the symmetric channel, Fig. 2(a), we can see that the key rate of asynchronous MDI-QKD with *click filtering* is always higher than that of asynchronous MDI-QKD without *click filtering* based on $[\mu_a, \mu_b]$ group. This is expected since the filtering operation corresponds to a higher number of valid pairs and smaller statistical fluctuations in the estimation process. And the key rate of asynchronous MDI-QKD with *click filtering* is higher than that of asynchronous MDI-QKD without *click filtering* based on four intensity groups at short and medium distances. At a fiber length of 300 km, the secret key rate obtained with *click filtering* is approximately 1.11 times the one without *click filtering* based on four intensity groups, and 1.29 times the one based on $[\mu_a, \mu_b]$ group. The same trend is observed for the asymmetric channel (Fig. 2(b)).

C. Asynchronous MDI-QKD Networks

We provide a figure about a scalable QKD network setup consisting of numerous users who may freely join or leave the network in Fig. 3. Each user node has an asymmetric channel connected to an untrusted relay, through which it can establish a QKD link to others. The users will adjust the sending intensities and corresponding probability values so that each link can obtain the optimal key rate. The experimental parameters used

TABLE II. Simulated secret key rates per second for asynchronous MDI-QKD, SNS-QKD with the AOPP method, and PM-QKD in the QKD network shown in Fig. 3 using the parameters in Table IV. The system clock frequency is 4 GHz and the transmission time is 22 hours. Here, link A-B represents that user A communicates with user B. The sending intensities and corresponding probabilities are selected by the users to obtain the optimal key rate for each link. Note that here we consider a 50% duty cycle for the TF-type protocols [57, 67, 70].

Link	A-B (A-E)	B-C (C-E)	B-D (D-E)	B-E	A-C	A-D	C-D
SKC ₀	5.77×10^3	4.80×10^3	1.45×10^4	2.30×10^3	1.21×10^4	3.64×10^4	3.03×10^4
Asynchronous MDI-QKD	1.47×10^4	1.36×10^4	2.05×10^4	9.46×10^3	2.36×10^4	4.04×10^4	3.56×10^4
SNS-QKD (AOPP)	1.18×10^4	1.09×10^4	1.64×10^4	7.53×10^3	1.78×10^4	3.05×10^4	2.72×10^4
PM-QKD	2.56×10^3	2.40×10^3	3.22×10^3	1.71×10^3	4.19×10^3	6.91×10^3	6.01×10^3

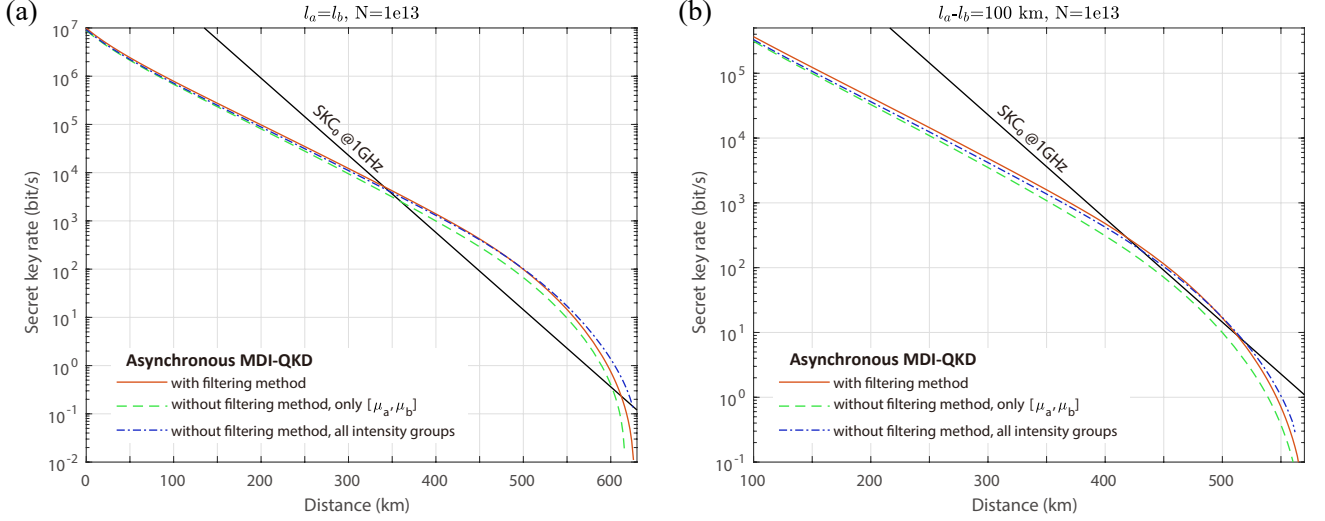


FIG. 2. Comparison of the secret key rates of asynchronous MDI-QKD with and without *click filtering* under two types of channels: (a) symmetric channel $l_a = l_b$ and (b) asymmetric channels $l_a - l_b = 100$ km.

here are listed in Table IV. We assume a 4 GHz clock rate [68] and 22-hour transmission time (about 3.2×10^{14} quantum pulses for asynchronous MDI-QKD).

Table II shows simulated secret key rates for asynchronous MDI-QKD, sending-or-not-sending QKD (SNS-QKD) with actively odd-parity pairing (AOPP) [82], and phase-matching QKD (PM-QKD) [83] in the QKD intercity network. We assume that the quantum transmission duty ratio of the SNS-QKD and PM-QKD systems is 50% [57, 67, 70]. Note that duty cycle ratios are lower in many important TF-QKD experiments, for example, the duty ratio at 402 km is 22.4% in Ref. [61], 45% in Ref. [62], and 40% in Ref. [68]. We can see that asynchronous MDI-QKD enables the key rates of all links to exceed SKC₀. Additionally, asynchronous MDI-QKD always enjoys higher secret key rates per clock than SNS-QKD (AOPP) and PM-QKD.

D. Practical advantages of asynchronous MDI-QKD

We simulate the performance of our protocol assuming a 4 GHz clock rate and 22 hours transmis-

sion time. Figure 4 presents the key rate per second versus fiber distance for asynchronous MDI-QKD, together with four-intensity time bin MDI-QKD [76], SNS-QKD (AOPP) [82], PM-QKD [83], four-phase TF-QKD [68], and four-intensity decoy-state QKD. For SNS-QKD (AOPP), PM-QKD, and four-phase TF-QKD, we set the duty cycle to 50%, Charlie's transmission loss at Alice's (Bob's) side to 2 dB, and the loss-independent misalignment error to 4.8% [70]. We assume an insert loss on Bob's side of 2 dB and a loss-independent misalignment error of $e_m = 0.02$ for decoy-state QKD. The interference misalignment error rate of decoy-state MDI-QKD is set to 0.04, which corresponds to 26% error rate in the X basis. Device parameters are shown in Table IV. The simulation formulas of MDI-QKD and decoy-state QKD are detailed in Appendix D 2 and D 3, respectively. We also include SKC₀ to prove the repeater-like behavior for asynchronous MDI-QKD. Simulation shows that the key rate of our protocol surpasses that of the decoy-state QKD protocol when $l > 170$ km, and it exceeds SKC₀ when $l > 330$ km. In the 170-483 km range, the performance of our protocol is better than that of the other five protocols, especially in the range of 200-300 km. We observe that, in the simulations, the key

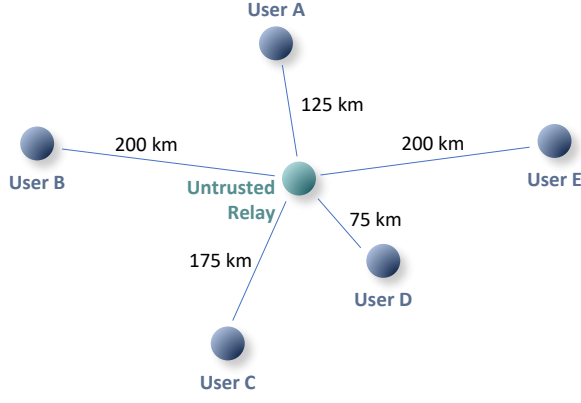


FIG. 3. Example of a scalable QKD network setup consisting of numerous users who may freely join or leave the network. Each user node has an asymmetric channel connected to an untrusted relay, through which it can establish a QKD link to others.

rates of decoy-state QKD surpass those of original time bin MDI-QKD due to the influence of the dark rate and finite key analysis. Within the 0-45km range, the original time bin MDI-QKD demonstrates a greater rate than asynchronous MDI-QKD. The lower key rate of asynchronous MDI-QKD at short distances (less than 45km) in comparison to the original time bin MDI-QKD is attributed to the stronger light intensity of the signal state in original MDI-QKD, approaching 1, which results in a higher number of single-photon pairs in the Z basis. In Table III, we present the bits-per-second (bps) values of asynchronous MDI-QKD at various typical distances, employing device parameters identical to those employed in Fig. 4. Our protocol can generate secret keys rate of 0.31 Mbps at a fiber length of 200 km, thereby rendering it adequate for secure key-demanding applications such as real-time one-time-pad secure audio encryption in intra- and inter-urban areas.

V. DISCUSSION AND CONCLUSION

Here, we point out two conceptual differences between asynchronous MDI-QKD and original MDI-QKD.

i. Coincidence pairing. In original MDI-QKD, the expected yields of single-photon pairs in the Z and X bases satisfy the relation $Y_{11}^{Z*} = Y_{11}^{X*}$ [31, 33]. However, since asynchronous MDI-QKD uses post-measurement coincidence pairing, there is no concept of the expected total pair number. Therefore, the ‘gain’ and ‘yield’ cannot be calculated.

ii. Overcompleteness. For asynchronous MDI-QKD, the so-called three-intensity and four-intensity refer to the number of light intensities sent, and the intensities at different bases after pairing are associated.

In the original MDI-QKD protocol, an important idea is to consider the double-scanning method [76]. We have

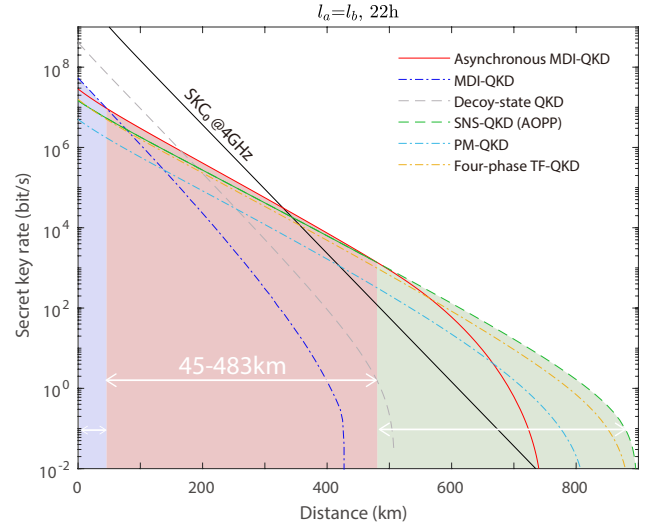


FIG. 4. Simulated secret key rates for asynchronous MDI-QKD, original time-bin MDI-QKD, decoy-state QKD, SNS-QKD with the AOOP method, PM-QKD, and four-phase TF-QKD under the state-of-the-art system.

applied the double-scanning method to asynchronous MDI-QKD. The derivation details of double-scanning are shown in Appendix B. However, numerical results show that the method does not work for the three-intensity asynchronous MDI-QKD protocol [84]. We remark that this phenomenon may be caused by the above two important characteristics. For three-intensity asynchronous MDI-QKD, there are three intensities in each of the Z and X bases after coincidence pairing. Whereas in the original three-intensity MDI-QKD, there is only one intensity in the Z basis. This means that we can directly use the Z -basis data to tightly estimate the number of single photon pairs in the Z basis for asynchronous MDI-QKD, rather than inefficiently using data from the X basis to calculate. Additionally, the overcompleteness of asynchronous MDI-QKD connotes that there is a correlation between the intensity used to estimate the number of the Z -basis single-photon pairs and the intensity used to estimate the X -basis phase error rate (Z basis: μ and ν ; X basis: 2μ and 2ν). In contrast, the intensity and decoy-state estimation for the Z and X bases are independent of original MDI-QKD, so double scanning is effective.

Furthermore, in the original MDI-QKD protocol, we can improve the performance of the protocol by increasing the number of decoy states, such as four-intensity MDI-QKD [31]. We also have calculated the key rate of the four-intensity asynchronous MDI-QKD protocol, in which the intensity of each laser pulse is randomly set to one of the four intensities $\mu_{a(b)}$ (signal), $\omega_{a(b)}$ (decoy 1), $\nu_{a(b)}$ (decoy 2) and $o_{a(b)}$ (vacuum), and the intensities satisfy $\mu_{a(b)} > \omega_{a(b)} > \nu_{a(b)} > o_{a(b)} = 0$. The detailed calculation of the protocol is presented in Appendix C. Comparing secret key rates of the three-intensity and

TABLE III. The secret key rates of the three-intensity asynchronous MDI-QKD protocol with *click filtering*. Here the fiber loss is 0.16 dB/km; the clock rate is 4 GHz; the dark count rates is 0.1 Hz; and the detection efficiency is $\eta_d = 80\%$.

Data size	10^{12}	5×10^{12}	10^{13}	10^{13}	5×10^{13}	5×10^{13}
Distance (km)	50	100	150	200	250	300
Secret key rate	6.02 Mbps	2.29 Mbps	855.40 kbps	305.05 kbps	129.60 kbps	46.671 kbps

four-intensity asynchronous MDI-QKD protocol with *click filtering*, we find that the optimal key rates for the four-intensity decoy-state method are nearly equal to the results for the three-intensity decoy-state method [84]. We remark that this situation is also due to overcompleteness. Therefore, the three-intensity asynchronous MDI-QKD protocol is a good trade-off between the performance of key rates and the ease of implementation.

In this work, we have presented an analysis of the practical aspects of asynchronous MDI-QKD. We have provided refined decoy-state methods that enable higher-rate asynchronous MDI-QKD. The numerical results of different asynchronous MDI-QKD protocols demonstrate that the three-intensity protocol, with a *click filtering* operation, can provide a favorable balance between performance and ease of implementation. We have introduced the decoy-state method for the asymmetric situation, which permits the direct application of our protocol to asynchronous MDI-QKD experiments with asymmetric channels. Our work also provides important insights into asynchronous MDI-QKD: the decoy-state analysis for the \mathbf{Z} and \mathbf{X} bases of asynchronous MDI-QKD are overcomplete, rendering the introduction of double scanning and additional decoy states ineffective for key rate improvement. With its superior performance and straightforward design, asynchronous MDI-QKD holds strong potential in future quantum networks spanning 200 to 400 km. We anticipate the application of the asynchronous concept to MDI multiparty quantum communication tasks, such as quantum conference key agreement [85], quantum secret sharing [85], and quantum digital signatures [86].

ACKNOWLEDGMENTS

The authors acknowledge Z. Yuan and L. Zhou for the insightful discussions. This work has been supported by the National Natural Science Foundation of China (No. 12274223), the Natural Science Foundation of Jiangsu Province (No. BK20211145), the Fundamental Research Funds for the Central Universities (No. 020414380182), the Key Research and Development Program of Nanjing Jiangbei New Area (No. ZDYD20210101), the Program for Innovative Talents and Entrepreneurs in Jiangsu (No. JSSCRC2021484), and the Program of Song Shan Laboratory (Included in the management of Major Science and Technology Program of Henan Province) (No. 221100210800).

Appendix A: Analytic results of joint constraints

Here, we introduce the joint-constraints method to bound tighter values. Without loss of generality, we take Eq. (6) as an example. Similar operations can be applied to other parameters. We can rewrite Eq. (6) as

$$\underline{S}_{11}^{z*} \geq \frac{\sum_{\tilde{k}_a, \tilde{k}_b} (\tilde{k}_a \tilde{k}_b e^{-\tilde{k}_a - \tilde{k}_b} p_{[\tilde{k}_a, \tilde{k}_b]})}{\nu_a \nu_b \mu_a \mu_b (\mu' - \nu')} (\underline{S}_1^* - \bar{S}_2^*), \quad (\text{A1})$$

where

$$\begin{aligned} S_1 = & \mu_a \mu_b \mu' e^{\nu_a + \nu_b} \frac{n_{[\nu_a, \nu_b]}}{p_{[\nu_a, \nu_b]}} + \nu_a \nu_b \nu' e^{\mu_b} \frac{n_{[o_a, \mu_b]}}{p_{[o_a, \mu_b]}} \\ & + \nu_a \nu_b \nu' e^{\mu_a} \frac{n_{[\mu_a, o_b]}}{p_{[\mu_a, o_b]}} + (\mu_a \mu_b \mu' - \nu_a \nu_b \nu') \frac{n_{[o_a, o_b]}}{p_{[o_a, o_b]}}, \end{aligned} \quad (\text{A2})$$

and

$$\begin{aligned} S_2 = & \nu_a \nu_b \nu' e^{\mu_a + \mu_b} \frac{n_{[\mu_a, \mu_b]}}{p_{[\mu_a, \mu_b]}} + \mu_a \mu_b \mu' e^{\nu_b} \frac{n_{[o_a, \nu_b]}^*}{p_{[o_a, \nu_b]}} \\ & + \mu_a \mu_b \mu' e^{\nu_a} \frac{n_{[\nu_a, o_b]}}{p_{[\nu_a, o_b]}}. \end{aligned} \quad (\text{A3})$$

For \underline{S}_1^* , we define

$$S_1 := a_1 \gamma_1 + a_2 \gamma_2 + a_3 \gamma_3 + a_4 \gamma_4, \quad (\text{A4})$$

where $a_1 = \frac{\mu_a \mu_b \mu' e^{\nu_a + \nu_b}}{p_{[\nu_a, \nu_b]}}$, $\gamma_1 = n_{[\nu_a, \nu_b]}$, $a_2 = \frac{\nu_a \nu_b \nu' e^{\mu_b}}{p_{[o_a, \mu_b]}}$, $\gamma_2 = n_{[o_a, \mu_b]}$, $a_3 = \frac{\nu_a \nu_b \nu' e^{\mu_a}}{p_{[\mu_a, o_b]}}$, $\gamma_3 = n_{[\mu_a, o_b]}$, $a_4 = \frac{\mu_a \mu_b \mu' - \nu_a \nu_b \nu'}{p_{[o_a, o_b]}}$, $\gamma_4 = n_{[o_a, o_b]}$. Denoting $\{b_1, b_2, b_3, b_4\}$ as the ascending order of $\{a_1, a_2, a_3, a_4\}$, and $\xi_1, \xi_2, \xi_3, \xi_4$ as the corresponding rearrange of $\{\gamma_1, \gamma_2, \gamma_3, \gamma_4\}$ according to the ascending order of $\{a_1, a_2, a_3, a_4\}$, then we have the lower bound of S_1^* [76]:

$$\begin{aligned} \underline{S}_1^* := & b_1 (\xi_1 + \xi_2 + \xi_3 + \xi_4)^* + (b_2 - b_1) (\xi_2 + \xi_3 + \xi_4)^* \\ & + (b_3 - b_2) (\xi_3 + \xi_4)^* + (b_4 - b_3) \xi_4^*. \end{aligned} \quad (\text{A5})$$

For \bar{S}_2^* , we define

$$S_2 := c_1 \kappa_1 + c_2 \kappa_2 + c_3 \kappa_3 + c_4 \kappa_4 \quad (\text{A6})$$

where $a_1 = \frac{\mu_a \mu_b \mu' e^{\nu_a + \nu_b}}{p_{[\nu_a, \nu_b]}}$, $\gamma_1 = n_{[\nu_a, \nu_b]}$, $a_2 = \frac{\nu_a \nu_b \nu' e^{\mu_b}}{p_{[o_a, \mu_b]}}$, $\gamma_2 = n_{[o_a, \mu_b]}$, $a_3 = \frac{\nu_a \nu_b \nu' e^{\mu_a}}{p_{[\mu_a, o_b]}}$, $\gamma_3 = n_{[\mu_a, o_b]}$, $a_4 = \frac{\mu_a \mu_b \mu' - \nu_a \nu_b \nu'}{p_{[o_a, o_b]}}$, $\gamma_4 = n_{[o_a, o_b]}$. Denoting $\{d_1, d_2, d_3\}$ as

the ascending order of $\{c_1, c_2, c_3\}$, and χ_2, χ_3 , as the corresponding rearrange of $\{\kappa_1, \kappa_2, \kappa_3\}$ according to the ascending order of $\{c_1, c_2, c_3\}$, then we have the upper bound of S_2^* [76]:

$$\begin{aligned} \bar{S}_2^* := & d_1 \times \overline{(\chi_1 + \chi_2 + \chi_3)}^* + (d_2 - d_1) \times \overline{(\chi_2 + \chi_3)}^* \\ & + (d_3 - d_2) \times \bar{\chi}_3^*. \end{aligned} \quad (\text{A7})$$

Appendix B: Decoy-state estimation with the double-scanning method

Here we apply the double-scanning method to asynchronous MDI-QKD. Using the decoy-state method, we can estimate the lower bound of the number of single-photon pairs in the \mathbf{X} basis

$$s_{11}^{x*} = \frac{e^{-2\nu_a - 2\nu_b} p_{[2\nu_a, 2\nu_b]}}{\mu_a \mu_b (\tilde{\mu}' - \tilde{\nu}')} (\underline{S}^{+*} - \bar{S}^{-*} - \bar{H}^*), \quad (\text{B1})$$

where

$$\begin{cases} \tilde{\mu}' = 2\mu_a, & \tilde{\nu}' = 2\nu_a, & \text{if } \frac{\mu_a}{\mu_b} \leq \frac{\nu_a}{\nu_b}, \\ \tilde{\mu}' = 2\mu_b, & \tilde{\nu}' = 2\nu_b, & \text{if } \frac{\mu_a}{\mu_b} > \frac{\nu_a}{\nu_b}, \end{cases} \quad (\text{B2})$$

and

$$\begin{aligned} S^{+*} = & \mu_a \mu_b \tilde{\mu}' e^{2\nu_a + 2\nu_b} \frac{n_{[2\nu_a, 2\nu_b]}^*}{p_{[2\nu_a, 2\nu_b]}} + \nu_a \nu_b \tilde{\nu}' e^{2\mu_b} \frac{n_{[o_a, 2\mu_b]}^*}{p_{[o_a, 2\mu_b]}} \\ & + \nu_a \nu_b \tilde{\nu}' e^{2\mu_a} \frac{n_{[2\mu_a, o_b]}^*}{p_{[2\mu_a, o_b]}}, \\ S^{-*} = & \nu_a \nu_b \tilde{\nu}' e^{2\mu_a + 2\mu_b} \frac{\bar{n}_{[2\mu_a, 2\mu_b]}^*}{p_{[2\mu_a, 2\mu_b]}} + \nu_a \nu_b \tilde{\nu}' e^{2\mu_b} \frac{\bar{n}_{[o_a, o_b]}^*}{p_{[o_a, o_b]}}, \\ H^* = & \mu_a \mu_b \tilde{\mu}' \left(e^{2\nu_b} \frac{n_{[o_a, 2\nu_b]}^*}{p_{[o_a, 2\nu_b]}} + e^{2\nu_a} \frac{n_{[2\nu_a, o_b]}^*}{p_{[2\nu_a, o_b]}} - \frac{\bar{n}_{[o_a, o_b]}^*}{p_{[o_a, o_b]}} \right). \end{aligned} \quad (\text{B3})$$

The upper bound of the bit error rate of single-photon pairs in the \mathbf{X} basis e_{11}^{x*} satisfies

$$\bar{e}_{11}^{x*} = \frac{1}{\mu_a \mu_b \tilde{\mu}' e^{2\nu_a + 2\nu_b} \underline{s}_{11}^{x*}} \left(\mu_a \mu_b \tilde{\mu}' e^{2\nu_a + 2\nu_b} \frac{m_{[2\nu_a, 2\nu_b]}^*}{p_{[2\nu_a, 2\nu_b]}} - \frac{H}{2} \right). \quad (\text{B4})$$

Denote $\tilde{n}_{[2\nu_a, 2\nu_b]} = n_{[2\nu_a, 2\nu_b]} - m_{[2\nu_a, 2\nu_b]}$. We can divide the effective $[2\nu_a, 2\nu_b]$ coincidence into two kinds of events, the right effective events whose total number is $\tilde{n}_{[2\nu_a, 2\nu_b]}$, and the wrong effective events whose total number is $m_{[2\nu_a, 2\nu_b]}$. Denote $M = \mu_a \mu_b \tilde{\mu}' e^{2\nu_a + 2\nu_b} \underline{m}_{[2\nu_a, 2\nu_b]}^* / p_{[2\nu_a, 2\nu_b]}$. We can rewrite Eq. (B1) as

$$\underline{s}_{11}^{x*} = \frac{e^{-2\nu_a - 2\nu_b} p_{[2\nu_a, 2\nu_b]}}{\mu_a \mu_b (\tilde{\mu}' - \tilde{\nu}')} (\tilde{\underline{S}}^{+*} - \bar{S}^{-*} + \underline{M}^* - \bar{H}^*), \quad (\text{B5})$$

where

$$\begin{aligned} \tilde{S}^{+*} = & \mu_a \mu_b \tilde{\mu}' e^{2\nu_a + 2\nu_b} \frac{\tilde{n}_{[2\nu_a, 2\nu_b]}^*}{p_{[2\nu_a, 2\nu_b]}} + \nu_a \nu_b \tilde{\nu}' e^{2\mu_b} \frac{n_{[o_a, 2\mu_b]}^*}{p_{[o_a, 2\mu_b]}} \\ & + \nu_a \nu_b \tilde{\nu}' e^{2\mu_a} \frac{n_{[2\mu_a, o_b]}^*}{p_{[2\mu_a, o_b]}}, \\ S^{-*} = & \nu_a \nu_b \tilde{\nu}' e^{2\mu_a + 2\mu_b} \frac{n_{[2\mu_a, 2\mu_b]}^*}{p_{[2\mu_a, 2\mu_b]}} + \nu_a \nu_b \tilde{\nu}' e^{2\mu_b} \frac{n_{[o_a, o_b]}^*}{p_{[o_a, o_b]}}, \\ H^* = & \mu_a \mu_b \tilde{\mu}' \left(e^{2\nu_b} \frac{n_{[o_a, 2\nu_b]}^*}{p_{[o_a, 2\nu_b]}} + e^{2\nu_a} \frac{n_{[2\nu_a, o_b]}^*}{p_{[2\nu_a, o_b]}} - \frac{n_{[o_a, o_b]}^*}{p_{[o_a, o_b]}} \right). \end{aligned} \quad (\text{B6})$$

For each group (H, M) , we can calculate e_{11}^{x*} with Eqs. (B4) and (B5)

$$\bar{e}_{11}^{x*} = \frac{(\tilde{\mu}' - \tilde{\nu}')(M - H/2)}{\tilde{\mu}'(S^+ - S^- + M - H)}. \quad (\text{B7})$$

By scanning (H, M) [76], we can get the worst case for e_{11}^{x*} , i.e.,

$$\max e_{11}^{x*} \quad (\text{B8})$$

$$\begin{aligned} \text{s.t. } & \underline{H} \leq H \leq \bar{H}, \\ & \underline{M} \leq M \leq \bar{M}. \end{aligned} \quad (\text{B9})$$

With the formulas in Eqs. (2), (3), (5), (6), and (13), we can get the final key rate.

Appendix C: Four-intensity asynchronous MDI-QKD protocol

Here, we provide the decoy-state method for four-intensity asynchronous MDI-QKD with *click filtering*. The core difference in the parameter estimation steps between the four-intensity protocol and the three-intensity protocol is to estimate the lower bound of the number of single-photon pairs in the \mathbf{Z} basis. In the four-intensity protocol with *click filtering*, s_{11}^{z*} is bounded by

$$\begin{aligned} \underline{s}_{11}^{z*} = & \frac{\sum_{\tilde{k}_a, \tilde{k}_b} (\tilde{k}_a \tilde{k}_b e^{-\tilde{k}_a - \tilde{k}_b} p_{[\tilde{k}_a, \tilde{k}_b]})}{\nu_a \nu_b \omega_a \omega_b (\omega' - \nu')} \\ & \times \left[\omega_a \omega_b \omega' \left(e^{\nu_a + \nu_b} \frac{n_{[\nu_a, \nu_b]}^*}{p_{[\nu_a, \nu_b]}} - e^{\nu_b} \frac{\bar{n}_{[o_a, \nu_b]}^*}{p_{[o_a, \nu_b]}} \right. \right. \\ & \left. \left. - e^{\nu_a} \frac{\bar{n}_{[\nu_a, o_b]}^*}{p_{[\nu_a, o_b]}} + \frac{n_{[o_a, o_b]}^*}{p_{[o_a, o_b]}} \right) \right. \\ & \left. - \nu_a \nu_b \nu' \left(e^{\omega_a + \omega_b} \frac{\bar{n}_{[\omega_a, \omega_b]}^*}{p_{[\omega_a, \omega_b]}} - e^{\omega_b} \frac{n_{[o_a, \omega_b]}^*}{p_{[o_a, \omega_b]}} \right. \right. \\ & \left. \left. - e^{\omega_a} \frac{n_{[\omega_a, o_b]}^*}{p_{[\omega_a, o_b]}} + \frac{n_{[o_a, o_b]}^*}{p_{[o_a, o_b]}} \right) \right], \end{aligned} \quad (\text{C1})$$

where

$$\begin{cases} \omega' = \omega_a, & \nu' = \nu_a & \text{if } \frac{\omega_a}{\omega_b} \leq \frac{\nu_a}{\nu_b}, \\ \omega' = \omega_b, & \nu' = \nu_b & \text{if } \frac{\omega_a}{\omega_b} > \frac{\nu_a}{\nu_b}, \end{cases} \quad (\text{C2})$$

and $p_{[k_a^{\text{tot}}, k_b^{\text{tot}}]}$ is defined in Eq. (4). When *click filtering* is not applied, $p_s = 1$, otherwise $p_s = 1 - p_{\mu_a}p_{\omega_b} - p_{\mu_a}p_{\nu_b} - p_{\omega_a}p_{\mu_b} - p_{\omega_a}p_{\nu_b} - p_{\nu_a}p_{\mu_b} - p_{\nu_a}p_{\omega_b}$. Similarly, we use the technique of joint constraints to get the tight estimated value of s_{11}^* . The calculation of the remaining parameter values can directly utilize Eqs. (2), (3), and (8) - (13).

Appendix D: Simulation formulas

The experimental parameters used for performance comparison of these protocols, asynchronous MDI-QKD, decoy-state QKD, SNS-QKD (AOPP), PM-QKD, and four-phase TF-QKD, are listed in Table IV.

1. Simulation formulas for asynchronous MDI-QKD

In asynchronous MDI-QKD, suppose Alice and Bob send intensities k_a and k_b with phase difference θ , the overall gain is given by [Eq. (C22) in Ref. [75]]

$$q_{(k_a|k_b)} = y_{(k_a|k_b)}^L I_0 \left(\eta_d^L \sqrt{\eta_a k_a \eta_b k_b} \right) + y_{(k_a|k_b)}^R I_0 \left(\eta_d^R \sqrt{\eta_a k_a \eta_b k_b} \right) - 2y_{(k_a|k_b)}^L y_{(k_a|k_b)}^R I_0 \left[(\eta_d^L - \eta_d^R) \sqrt{\eta_a k_a \eta_b k_b} \right], \quad (\text{D1})$$

where $y_{(k_a|k_b)}^{L(R)} = \left(1 - p_d^{L(R)} \right) e^{-\frac{\eta_d^{L(R)} (\eta_a k_a + \eta_b k_b)}{2}}$; η_d^L (η_d^R) and p_d^L (p_d^R) are the detection efficiency and the dark count rate of the detector D_L (D_R), respectively; $\eta_a = 10^{-\frac{\alpha l_a}{10}}$ and $\eta_b = 10^{-\frac{\alpha l_b}{10}}$; $I_0(x)$ refers to the zero-order modified Bessel function of the first kind.

We define $N_{T_c} = FT_c$ as the number of time bins within time interval T_c . The total number of valid successful pairing results is [Eq. (C24) in Ref. [75]]

$$n_{\text{tot}} = \frac{N q_{\text{tot}}}{1 + 1/q_{T_c}}, \quad (\text{D2})$$

where q_{tot} is the probability of having a click event, and $q_{T_c} = 1 - (1 - q_{\text{tot}})^{N_{T_c}}$ is the probability that at least one click event occurs within the time interval T_c after a click time bin. When using the matching method without click filtering, $q_{\text{tot}} = \sum_{k_a, k_b} p_{k_a} p_{k_b} q_{(k_a|k_b)}$; when using the matching method with click filtering, $q_{\text{tot}} = \sum_{k_a, k_b} p_{k_a} p_{k_b} q_{(k_a|k_b)} - p_{\mu_a} p_{\nu_b} q_{(\mu_a|\nu_b)} - p_{\nu_a} p_{\mu_b} q_{(\nu_a|\mu_b)}$. The average of the pairing interval can be given by [Eq. (C25) in Ref. [75]]

$$T_{\text{mean}} = \frac{1 - N_{T_c} q_{\text{tot}} (1/q_{T_c} - 1)}{F q_{\text{tot}}}. \quad (\text{D3})$$

The total number of set $\mathcal{S}_{[k_a^{\text{tot}}, k_b^{\text{tot}}]}$ (except set $\mathcal{S}_{[2\nu_a, 2\nu_b]}$)

is [Eq. (C26) in Ref. [75]]

$$n_{[k_a^{\text{tot}}, k_b^{\text{tot}}]} = n_{\text{tot}} \times \sum_{k_a^e + k_a^l = k_a^{\text{tot}}} \sum_{k_b^e + k_b^l = k_b^{\text{tot}}} \left(\frac{p_{k_a^e} p_{k_b^e} q_{(k_a^e|k_b^e)}}{q_{\text{tot}}} \frac{p_{k_a^l} p_{k_b^l} q_{(k_a^l|k_b^l)}}{q_{\text{tot}}} \right). \quad (\text{D4})$$

The total number of set $\mathcal{S}_{[2\nu_a, 2\nu_b]}$ is [Eq. (C27) in Ref. [75]]

$$n_{[2\nu_a, 2\nu_b]} = \frac{n_{\text{tot}}}{M\pi} \int_0^{2\pi} \left(\frac{p_{\nu_a} p_{\nu_b} q_{(\nu_a|\nu_b)}^\theta}{q_{\text{tot}}} \frac{p_{\nu_a} p_{\nu_b} q_{(\nu_a|\nu_b)}^\theta}{q_{\text{tot}}} \right) d\theta. \quad (\text{D5})$$

The total number of errors in the \mathbf{X} basis can be written as [Eq. (C28) in Ref. [75]]

$$m_{[2\nu_a, 2\nu_b]} = \frac{n_{\text{tot}}}{M\pi} p_{\nu_a}^2 p_{\nu_b}^2 \times \int_0^{2\pi} \left\{ (1 - E_{\text{HOM}}) \frac{[q_{(\nu_a|\nu_b)}^{\theta, L} q_{(\nu_a|\nu_b)}^{\theta+\delta, R} + q_{(\nu_a|\nu_b)}^{\theta, R} q_{(\nu_a|\nu_b)}^{\theta+\delta, L}]}{q_{\text{tot}}^2} + E_{\text{HOM}} \frac{[q_{(\nu_a|\nu_b)}^{\theta, L} q_{(\nu_a|\nu_b)}^{\theta+\delta, L} + q_{(\nu_a|\nu_b)}^{\theta, R} q_{(\nu_a|\nu_b)}^{\theta+\delta, R}]}{q_{\text{tot}}^2} \right\} d\theta, \quad (\text{D6})$$

where E_{HOM} is the interference misalignment error rate, and $\delta = T_{\text{mean}}(2\pi\Delta\nu + \omega_{\text{fb}})$ is the phase misalignment resulting from the fiber phase drift rate ω_{fb} and laser frequency difference $\Delta\nu$.

2. Simulation formulas for four-intensity MDI-QKD

We denote the number and error number of detection event when Alice sends intensity k_a ($k_a \in \{\mu_a, \nu_a, \omega_a, o_a\}$), and Bob sends k_b ($k_b \in \{\mu_b, \nu_b, \omega_b, o_b\}$) in the $\mathbf{Z}(\mathbf{X})$ basis as $n_{k_a k_b}^{z(x)}$ and $m_{k_a k_b}^{z(x)}$, respectively. The key rate of time-bin MDI-QKD is [29, 76]

$$R = \frac{1}{N'} \left\{ \bar{n}_0^z + \bar{n}_{11}^z \left[1 - H_2 \left(\bar{\phi}_{11}^z \right) \right] - \lambda_{\text{EC}} - \log_2 \frac{2}{\varepsilon_{\text{cor}}} - 2 \log_2 \frac{2}{\varepsilon' \bar{\varepsilon}} - 2 \log_2 \frac{1}{2\varepsilon_{\text{PA}}} \right\}, \quad (\text{D7})$$

where $\lambda_{\text{EC}} = n_{\mu_a \mu_b}^z f H_2 \left(\frac{m_{\mu_a \mu_b}^z}{n_{\mu_a \mu_b}^z} \right)$.

Here we use the decoy-state analysis to consider the complete finite-key effects and apply the double-scanning method to MDI-QKD [76]. The corresponding parame-

TABLE IV. List of experimental parameters used in numerical simulations.

	Asynchronous MDI-QKD	Decoy-state QKD	SNS-QKD & PM-QKD	Four-phase TF-QKD
Fiber loss	0.16 dB/km	0.16 dB/km	0.16 dB/km	0.16 dB/km
Charlie loss	—	2 dB	—	—
Detector efficiency	80%	80%	80%	80%
Dark count rate	0.1 Hz	0.1 Hz	0.1 Hz	0.1 Hz
Spectral filtering loss	0 dB	0 dB	2 dB at Alice-Charlie 2 dB at Bob-Charlie	2 dB at Alice-Charlie 2 dB at Bob-Charlie
Duty Cycle	100	100	50	50
Laser frequency difference	10 Hz	—	—	—
Drift rates	5.9×10^3 rad/s	—	—	—
Number of phase slices	16	—	16	4

ters in Eq. (D7) can be given by

$$\begin{aligned}
n_0^{z*} &= \max \left\{ \frac{e^{-\mu_a} p_{\mu_a}}{p_{o_a}} \underline{n}_{o_a \mu_b}^{z*}, \frac{e^{-\mu_b} p_{\mu_b}}{p_{o_b}} \underline{n}_{\mu_a o_b}^{z*} \right\}, \\
\underline{n}_{11}^{z*} &= \frac{\mu_a \mu_b e^{-\mu_a - \mu_b} p_{\mu_a} p_{\mu_b}}{\nu_a \nu_b \omega_a \omega_b (\omega' - \nu')} \left(\underline{P}^{+*} - \overline{P}^{-*} + \underline{\hat{M}}^* - \widehat{H}^* \right), \\
\bar{t}_{11}^{x*} &= \frac{1}{\omega_a \omega_b \omega' e^{\nu_a + \nu_b}} \left(\hat{M} - \frac{\hat{H}}{2} \right), \\
\bar{t}_{11}^{z*} &= \frac{\mu_a \mu_b e^{-\mu_a - \mu_b} p_{\mu_a} p_{\mu_b}}{\nu_a \nu_b e^{-\nu_a - \nu_b} p_{\nu_a} p_{\nu_b}} \bar{t}_{11}^{x*}, \\
\bar{\phi}_{11}^z &= \frac{\bar{t}_{11}^{z*}}{\underline{n}_{11}^{z*}},
\end{aligned} \tag{D8}$$

where

$$\begin{cases} \omega' = \omega_a, & \nu' = \nu_a & \text{if } \frac{\omega_a}{\omega_b} \leq \frac{\nu_a}{\nu_b}, \\ \omega' = \omega_b, & \nu' = \nu_b & \text{if } \frac{\omega_a}{\omega_b} > \frac{\nu_a}{\nu_b}. \end{cases} \tag{D9}$$

and

$$\begin{aligned}
P^{+*} &= \omega_a \omega_b \omega' e^{\nu_a + \nu_b} \frac{(\underline{n}_{\nu_a \nu_b}^x - m_{\nu_a \nu_b}^x)^*}{p_{\nu_a} p_{\nu_b}} \\
&\quad + \nu_a \nu_b \nu' e^{\omega_a + \omega_b} \frac{n_{\omega_a \omega_b}^{x*}}{p_{\omega_a} p_{\omega_b}} + \nu_a \nu_b \nu' e^{\omega_b} \frac{n_{o_a \omega_b}^{x*}}{p_{o_a} p_{\omega_b}}, \\
P^{-*} &= \nu_a \nu_b \nu' e^{\omega_a + \omega_b} \frac{n_{\omega_a \omega_b}^{x*}}{p_{\omega_a} p_{\omega_b}} + \nu_a \nu_b \nu' \frac{n_{o_a o_b}^{x*}}{p_{o_a} p_{o_b}}, \\
\hat{M}^* &= \omega_a \omega_b \omega' e^{\nu_a + \nu_b} \frac{m_{\nu_a \nu_b}^{x*}}{p_{\nu_a} p_{\nu_b}}, \\
\hat{H}^* &= \omega_a \omega_b \omega' \left(e^{\nu_b} \frac{n_{o_a \nu_b}^{x*}}{p_{o_a} p_{\nu_b}} + e^{\nu_a} \frac{n_{\nu_a o_b}^{x*}}{p_{\nu_a} p_{o_b}} - \frac{n_{o_a o_b}^{x*}}{p_{o_a} p_{o_b}} \right).
\end{aligned} \tag{D10}$$

By scanning (\hat{H}, \hat{M}) , we can obtain the secret key rate

$$\min R \tag{D11}$$

$$\text{s.t. } \underline{\hat{H}} \leq \hat{H} \leq \overline{\hat{H}}, \tag{D12}$$

$$\underline{\hat{M}} \leq \hat{M} \leq \overline{\hat{M}}.$$

Because of the dead time of the detector, only one of the four Bell states can be identified. In the simulation, we set

$$\begin{aligned}
n_{k_a k_b}^z &= N' p_{k_a} p_{k_b} p_d (1 - p_d)^2 e^{-\frac{k_a \eta_a + k_b \eta_b}{2}} \\
&\quad \left\{ I_0(\sqrt{k_a \eta_a k_b \eta_b}) - (1 - p_d) e^{-\frac{k_a \eta_a + k_b \eta_b}{2}} \right. \\
&\quad \left. + \left[1 - (1 - p_d) e^{-\frac{k_a \eta_a}{2}} \right] \left[1 - (1 - p_d) e^{-\frac{k_b \eta_b}{2}} \right] \right\}, \\
m_{k_a k_b}^z &= N' p_{k_a} p_{k_b} p_d (1 - p_d)^2 e^{-\frac{k_a \eta_a + k_b \eta_b}{2}} \\
&\quad \left\{ \left[I_0(\sqrt{k_a \eta_a k_b \eta_b}) - (1 - p_d) e^{-\frac{k_a \eta_a + k_b \eta_b}{2}} \right] \right\},
\end{aligned} \tag{D13}$$

and

$$\begin{aligned}
n_{k_a k_b}^x &= N' p_{k_a} p_{k_b} y_{k_a k_b}^2 \left[1 + 2 y_{k_a k_b}^2 \right. \\
&\quad \left. - 4 y_{k_a k_b} I_0 \left(\frac{\sqrt{k_a \eta_a k_b \eta_b}}{2} \right) + I_0(\sqrt{k_a \eta_a k_b \eta_b}) \right], \\
m_{k_a k_b}^x &= N' p_{k_a} p_{k_b} y_{k_a k_b}^2 \left\{ 1 + y_{k_a k_b}^2 \right. \\
&\quad \left. - 2 y_{k_a k_b} I_0 \left(\frac{\sqrt{k_a \eta_a k_b \eta_b}}{2} \right) \right. \\
&\quad \left. + E_{\text{HOM}} \left[I_0(\sqrt{k_a \eta_a k_b \eta_b}) - 1 \right] \right\},
\end{aligned} \tag{D14}$$

where we have $y_{k_a k_b} = (1 - p_d) e^{-\frac{k_a \eta_a + k_b \eta_b}{4}}$ and $E_{\text{HOM}} = 0.04$. Note that in time-bin MDI-QKD, two pulses form one bit, i.e., $N' = N/2$.

3. Simulation formulas for four-intensity decoy-state QKD

The key rate of decoy-state QKD is [81, 87]

$$\begin{aligned}
R &= \frac{1}{N} \left\{ \underline{n}_0^z + \underline{n}_1^z \left[1 - H_2 \left(\bar{\phi}_1^z \right) \right] - \lambda_{\text{EC}} \right. \\
&\quad \left. - 6 \log_2 \frac{23}{\varepsilon_{\text{sec}}} - 2 \log_2 \frac{2}{\varepsilon_{\text{cor}}} \right\},
\end{aligned} \tag{D15}$$

where $\lambda_{\text{EC}} = (\underline{n}_\mu^z + \underline{n}_\nu^z) f H_2 \left(\frac{m_\mu^z + m_\nu^z}{\underline{n}_\mu^z + \underline{n}_\nu^z} \right)$, and $\underline{n}_k^{(x)}$ and $m_k^{(x)}$ are the number and error number of intensity pulse k ($k \in \{\mu, \nu, \omega, o\}$) measured in the $\mathbf{Z}(\mathbf{X})$ basis, respectively.

First, we extend the decoy state analysis to finite-size cases. The number of vacuum events in the \mathbf{Z} and \mathbf{X} bases satisfy

$$\underline{n}_0^{z*} = \frac{p_\mu e^{-\mu} + p_\nu e^{-\nu}}{p_o} \underline{n}_o^{z*}, \quad (\text{D16})$$

and

$$\underline{n}_0^{x*} = \frac{p_\omega e^{-\omega}}{p_o} \underline{n}_o^{x*}, \quad (\text{D17})$$

respectively.

The number of single-photon events in the \mathbf{Z} and \mathbf{X} bases are

$$\underline{n}_1^{z*} = \frac{(p_\mu \mu e^{-\mu} + p_\nu \nu e^{-\nu}) \mu}{\mu \nu - \nu^2} \left(\frac{e^\nu \underline{n}_\nu^{z*}}{p_\nu} - \frac{\nu^2}{\mu^2} \frac{e^\mu \bar{n}_\mu^{z*}}{p_\mu} - \frac{\mu^2 - \nu^2}{\mu^2} \frac{\bar{n}_o^{z*}}{p_o} \right), \quad (\text{D18})$$

and

$$\underline{n}_1^{x*} = \frac{p_\omega \omega e^{-\omega} \mu}{\mu \nu - \nu^2} \left(\frac{e^\nu \underline{n}_\nu^{x*}}{p_\nu} - \frac{\nu^2}{\mu^2} \frac{e^\mu \bar{n}_\mu^{x*}}{p_\mu} - \frac{\mu^2 - \nu^2}{\mu^2} \frac{\bar{n}_o^{x*}}{p_o} \right), \quad (\text{D19})$$

respectively. In addition, the number of bit errors \bar{t}_1^x associated with the single-photon events in the \mathbf{X} basis is also required. It is given by

$$\bar{t}_1^x = m_\omega^x - \underline{m}_0^x, \quad (\text{D20})$$

where $\underline{m}_0^{x*} = \frac{p_\omega e^{-\omega}}{p_o} \underline{m}_o^{x*}$. Second, the formula for the phase error rate of the single-photon events in the \mathbf{Z} basis can be written as

$$\bar{\phi}_1^z = \frac{\bar{m}_1^x}{\underline{n}_1^x} + \gamma \left(\underline{n}_1^z, \underline{n}_1^x, \frac{\bar{t}_1^x}{\underline{n}_1^x}, \varepsilon_e \right). \quad (\text{D21})$$

In the simulation, we set

$$\begin{aligned} n_k^z &= \frac{N p_k}{2} \left[1 - (1 - p_d^z)^2 e^{-k q_z \eta^z} \right] \left[1 + (1 - p_d^x)^2 e^{-k q_x \eta^x} \right], \\ m_k^z &= \frac{N p_k}{2} \left[1 + (1 - p_d^x)^2 e^{-k q_x \eta^x} \right] \left\{ (e_0 - e_m^z) \left[1 - (1 - p_d^z)^2 \right] e^{-k q_z \eta^z} + e_m^z \left[1 - (1 - p_d^z)^2 e^{-k q_z \eta^z} \right] \right\}, \end{aligned} \quad (\text{D22})$$

and

$$\begin{aligned} n_k^x &= \frac{N p_k}{2} \left[1 - (1 - p_d^x)^2 e^{-k q_x \eta^x} \right] \left[1 + (1 - p_d^z)^2 e^{-k q_z \eta^z} \right], \\ m_k^x &= \frac{N p_k}{2} \left[1 + (1 - p_d^z)^2 e^{-k q_z \eta^z} \right] \left\{ (e_0 - e_m^x) \left[1 - (1 - p_d^x)^2 \right] e^{-k q_x \eta^x} + e_m^x \left[1 - (1 - p_d^x)^2 e^{-k q_x \eta^x} \right] \right\}, \end{aligned} \quad (\text{D23})$$

where $e_0 = 1/2$ is the error rate of the background noise, $e_m^z = e_m^x = e_m$, $p_d^z = p_d^x = p_d$, and $\eta^z = \eta^x = \eta_d 10^{-\frac{\alpha l + \eta_{\text{int}}}{10}}$. The code of decoy-state QKD and decoy-state MDI-QKD has been uploaded to the open-source code website [84].

Appendix E: Statistical fluctuation analysis

value

$$\bar{x} = \varphi^U(x^*) = x^* + \frac{\beta}{2} + \sqrt{2\beta x^* + \frac{\beta^2}{4}}, \quad (\text{E1})$$

In this Appendix, we introduce the statistical fluctuation analysis method [81] used in the simulation.

and

$$\underline{x} = \varphi^L(x^*) = x^* - \sqrt{2\beta x^*}, \quad (\text{E2})$$

Chernoff bound. For a given expected value x^* and failure probability ε , we can use the Chernoff bound to estimate the upper and lower bounds of the observed

where $\beta = \ln \varepsilon^{-1}$.

Variant of Chernoff bound. The variant of the Chernoff bound can help us estimate the expected value from their observed values. One can apply the following equations to obtain the upper and lower bounds of x^*

$$\bar{x}^* = x + \beta + \sqrt{2\beta x + \beta^2}, \quad (\text{E3})$$

and

$$\underline{x}^* = \max \left\{ x - \frac{\beta}{2} - \sqrt{2\beta x + \frac{\beta^2}{4}}, 0 \right\}. \quad (\text{E4})$$

-
- [1] C. H. Bennett and G. Brassard, *Theor. Comput. Sci.* **560**, 7 (2014).
- [2] A. K. Ekert, *Phys. Rev. Lett.* **67**, 661 (1991).
- [3] V. Scarani, H. Bechmann-Pasquinucci, N. J. Cerf, M. Dušek, N. Lütkenhaus, and M. Peev, *Reviews of modern physics* **81**, 1301 (2009).
- [4] F. Xu, X. Ma, Q. Zhang, H.-K. Lo, and J.-W. Pan, *Rev. Mod. Phys.* **92**, 025002 (2020).
- [5] S. Pirandola, U. L. Andersen, L. Banchi, M. Berta, D. Bunandar, R. Colbeck, D. Englund, T. Gehring, C. Lupo, C. Ottaviani, *et al.*, *Adv. Opt. Photon.* **12**, 1012 (2020).
- [6] F. Grünenfelder, A. Boaron, M. Perrenoud, G. V. Resta, D. Rusca, C. Barreiro, R. Houlmann, R. Sax, L. Stasi, S. El-Khoury, E. Hänggi, N. Bosshard, F. Bussi eres, and H. Zbinden, *arXiv preprint arXiv:2210.16126* (2022).
- [7] C. Gobby, a. Yuan, and A. Shields, *Appl. Phys. Lett.* **84**, 3762 (2004).
- [8] B. Fr hlich, M. Lucamarini, J. F. Dynes, L. C. Comandar, W. W.-S. Tam, A. Plews, A. W. Sharpe, Z. Yuan, and A. J. Shields, *Optica* **4**, 163 (2017).
- [9] A. Boaron, G. Boso, D. Rusca, C. Vulliez, C. Autebert, M. Caloz, M. Perrenoud, G. Gras, F. Bussi eres, M.-J. Li, D. Nolan, A. Martin, and H. Zbinden, *Phys. Rev. Lett.* **121**, 190502 (2018).
- [10] M. Peev, C. Pacher, R. All eume, C. Barreiro, J. Bouda, W. Boxleitner, T. Debuisschert, E. Diamanti, M. Dianati, J. F. Dynes, S. Fasel, S. Fossier, M. F rst, J.-D. Gautier, O. Gay, N. Gisin, P. Grangier, A. Happe, Y. Hasani, M. Hentschel, H. H bel, G. Humer, T. L nger, M. L gr , R. Lieger, J. Lodewyck, T. Lor nser, N. L tkenhaus, A. Marhold, T. Matyus, O. Maurhart, L. Monat, S. Nauerth, J.-B. Page, A. Poppe, E. Querasser, G. Ribordy, S. Robyr, L. Salvail, A. W. Sharpe, A. J. Shields, D. Stucki, M. Suda, C. Tamas, T. Themel, R. T. Thew, Y. Thoma, A. Treiber, P. Trinkler, R. Tualle-Brouiri, F. Vannel, N. Walenta, H. Weier, H. Weinfurter, I. Wimberger, Z. L. Yuan, H. Zbinden, and A. Zeilinger, *New J. Phys.* **11**, 075001 (2009).
- [11] M. Sasaki, M. Fujiwara, H. Ishizuka, W. Klaus, K. Wakui, M. Takeoka, S. Miki, T. Yamashita, Z. Wang, A. Tanaka, K. Yoshino, Y. Nambu, S. Takahashi, A. Tajima, A. Tomita, T. Domeki, T. Hasegawa, Y. Sakai, H. Kobayashi, T. Asai, K. Shimizu, T. Tokura, T. Tsurumaru, M. Matsui, T. Honjo, K. Tamaki, H. Takesue, Y. Tokura, J. F. Dynes, A. R. Dixon, A. W. Sharpe, Z. L. Yuan, A. J. Shields, S. Uchikoga, M. L gr , S. Robyr, P. Trinkler, L. Monat, J.-B. Page, G. Ribordy, A. Poppe, A. Allacher, O. Maurhart, T. L nger, M. Peev, and A. Zeilinger, *Opt. Express* **19**, 10387 (2011).
- [12] J. Dynes, A. Wonfor, W.-S. Tam, A. Sharpe, R. Takahashi, M. Lucamarini, A. Plews, Z. Yuan, A. Dixon, J. Cho, *et al.*, *npj Quantum Inf.* **5**, 101 (2019).
- [13] Y.-A. Chen, Q. Zhang, T.-Y. Chen, W.-Q. Cai, S.-K. Liao, J. K. Chen, J. Yin, J.-G. Ren, Z. Chen, S.-L. Han, Q. Yu, K. Liang, F. Zhou, X. Yuan, M.-S. Zhao, T.-Y. Wang, X. Jiang, L. Zhang, W.-Y. Liu, Y. Li, Q. Shen, Y. Cao, C.-Y. Lu, R. Shu, J.-Y. Wang, L. Li, N.-L. Liu, F. Xu, X.-B. Wang, C.-Z. Peng, and J.-W. Pan, *Nature* **589**, 214 (2021).
- [14] Y. Zhao, C.-H. F. Fung, B. Qi, C. Chen, and H.-K. Lo, *Phys. Rev. A* **78**, 042333 (2008).
- [15] L. Lydersen, C. Wiechers, C. Wittmann, D. Elser, J. Skaar, and V. Makarov, *Nat. Photonics* **4**, 686 (2010).
- [16] Y.-L. Tang, H.-L. Yin, X. Ma, C.-H. F. Fung, Y. Liu, H.-L. Yong, T.-Y. Chen, C.-Z. Peng, Z.-B. Chen, and J.-W. Pan, *Phys. Rev. A* **88**, 022308 (2013).
- [17] H.-K. Lo, M. Curty, and B. Qi, *Phys. Rev. Lett.* **108**, 130503 (2012).
- [18] S. L. Braunstein and S. Pirandola, *Phys. Rev. Lett.* **108**, 130502 (2012).
- [19] Y. Liu, T.-Y. Chen, L.-J. Wang, H. Liang, G.-L. Shentu, J. Wang, K. Cui, H.-L. Yin, N.-L. Liu, L. Li, X. Ma, J. S. Pelc, M. M. Fejer, C.-Z. Peng, Q. Zhang, and J.-W. Pan, *Phys. Rev. Lett.* **111**, 130502 (2013).
- [20] A. Rubenok, J. A. Slater, P. Chan, I. Lucio-Martinez, and W. Tittel, *Phys. Rev. Lett.* **111**, 130501 (2013).
- [21] Z. Tang, Z. Liao, F. Xu, B. Qi, L. Qian, and H.-K. Lo, *Phys. Rev. Lett.* **112**, 190503 (2014).
- [22] H.-L. Yin, T.-Y. Chen, Z.-W. Yu, H. Liu, L.-X. You, Y.-H. Zhou, S.-J. Chen, Y. Mao, M.-Q. Huang, W.-J. Zhang, H. Chen, M. J. Li, D. Nolan, F. Zhou, X. Jiang, Z. Wang, Q. Zhang, X.-B. Wang, and J.-W. Pan, *Phys. Rev. Lett.* **117**, 190501 (2016).
- [23] L. Comandar, M. Lucamarini, B. Fr hlich, J. Dynes, A. Sharpe, S.-B. Tam, Z. Yuan, R. Pentz, and A. Shields, *Nat. Photonics* **10**, 312 (2016).
- [24] H.-L. Yin, W.-L. Wang, Y.-L. Tang, Q. Zhao, H. Liu, X.-X. Sun, W.-J. Zhang, H. Li, I. V. Puthoor, L.-X. You, *et al.*, *Phys. Rev. A* **95**, 042338 (2017).
- [25] R. I. Woodward, Y. Lo, M. Pittaluga, M. Minder, T. Para so, M. Lucamarini, Z. Yuan, and A. Shields, *npj Quantum Inf.* **7**, 58 (2021).
- [26] H. Semenenko, P. Sibson, A. Hart, M. G. Thompson, J. G. Rarity, and C. Erven, *Optica* **7**, 238 (2020).
- [27] X. Zheng, P. Zhang, R. Ge, L. Lu, G. He, Q. Chen, F. Qu, L. Zhang, X. Cai, Y. Lu, S. Zhu, P. Wu, and X.-S. Ma, *Adv. Photonics* **3**, 055002 (2021).
- [28] K. Wei, W. Li, H. Tan, Y. Li, H. Min, W.-J. Zhang, H. Li, L. You, Z. Wang, X. Jiang, T.-Y. Chen, S.-K. Liao, C.-Z. Peng, F. Xu, and J.-W. Pan, *Phys. Rev. X* **10**, 031030 (2020).
- [29] M. Curty, F. Xu, W. Cui, C. C. W. Lim, K. Tamaki, and H.-K. Lo, *Nat. Commun.* **5**, 3732 (2014).
- [30] H.-L. Yin, W.-F. Cao, Y. Fu, Y.-L. Tang, Y. Liu, T.-Y. Chen, and Z.-B. Chen, *Opt. Lett.* **39**, 5451 (2014).

- [31] Y.-H. Zhou, Z.-W. Yu, and X.-B. Wang, *Phys. Rev. A* **93**, 042324 (2016).
- [32] C. Wang, Z.-Q. Yin, S. Wang, W. Chen, G.-C. Guo, and Z.-F. Han, *Optica* **4**, 1016 (2017).
- [33] W. Wang, F. Xu, and H.-K. Lo, *Phys. Rev. X* **9**, 041012 (2019).
- [34] K. Azuma, S. E. Economou, D. Elkouss, P. Hilaire, L. Jiang, H.-K. Lo, and I. Tzitrin, *arXiv preprint arXiv:2212.10820* (2022).
- [35] C. Zhang, X.-L. Hu, C. Jiang, J.-P. Chen, Y. Liu, W. Zhang, Z.-W. Yu, H. Li, L. You, Z. Wang, X.-B. Wang, Q. Zhang, and J.-W. Pan, *Phys. Rev. Lett.* **128**, 190503 (2022).
- [36] J. Gu, X.-Y. Cao, Y. Fu, Z.-W. He, Z.-J. Yin, H.-L. Yin, and Z.-B. Chen, *Science Bulletin* **67**, 2167 (2022).
- [37] S. Pirandola, R. García-Patrón, S. L. Braunstein, and S. Lloyd, *Phys. Rev. Lett.* **102**, 050503 (2009).
- [38] M. Takeoka, S. Guha, and M. M. Wilde, *Nat. Commun.* **5**, 5235 (2014).
- [39] S. Pirandola, R. Laurenza, C. Ottaviani, and L. Banchi, *Nat. Commun.* **8**, 15043 (2017).
- [40] S. Das, S. Bäuml, M. Winczewski, and K. Horodecki, *Phys. Rev. X* **11**, 041016 (2021).
- [41] L. Jiang, J. M. Taylor, K. Nemoto, W. J. Munro, R. Van Meter, and M. D. Lukin, *Phys. Rev. A* **79**, 032325 (2009).
- [42] W. J. Munro, A. M. Stephens, S. J. Devitt, K. A. Harrison, and K. Nemoto, *Nature Photonics* **6**, 777 (2012).
- [43] K. Azuma, K. Tamaki, and H.-K. Lo, *Nature communications* **6**, 1 (2015).
- [44] K. Azuma, K. Tamaki, and W. J. Munro, *Nat. Commun.* **6**, 10171 (2015).
- [45] M. Lucamarini, Z. L. Yuan, J. F. Dynes, and A. J. Shields, *Nature* **557**, 400 (2018).
- [46] X. Ma, P. Zeng, and H. Zhou, *Phys. Rev. X* **8**, 031043 (2018).
- [47] X.-B. Wang, Z.-W. Yu, and X.-L. Hu, *Phys. Rev. A* **98**, 062323 (2018).
- [48] H.-L. Yin and Y. Fu, *Sci. Rep.* **9**, 3045 (2019).
- [49] J. Lin and N. Lütkenhaus, *Phys. Rev. A* **98**, 042332 (2018).
- [50] C. Cui, Z.-Q. Yin, R. Wang, W. Chen, S. Wang, G.-C. Guo, and Z.-F. Han, *Phys. Rev. Applied* **11**, 034053 (2019).
- [51] M. Curty, K. Azuma, and H.-K. Lo, *npj Quantum Inf.* **5**, 64 (2019).
- [52] K. Maeda, T. Sasaki, and M. Koashi, *Nat. Commun.* **10**, 3140 (2019).
- [53] H.-L. Yin and Z.-B. Chen, *Sci. Rep.* **9**, 17113 (2019).
- [54] C. Jiang, Z.-W. Yu, X.-L. Hu, and X.-B. Wang, *Phys. Rev. Applied* **12**, 024061 (2019).
- [55] G. Currás-Lorenzo, Á. Navarrete, K. Azuma, G. Kato, M. Curty, and M. Razavi, *npj Quantum Inf.* **7**, 22 (2021).
- [56] B.-H. Li, Y.-M. Xie, Z. Li, C.-X. Weng, C.-L. Li, H.-L. Yin, and Z.-B. Chen, *Opt. Lett.* **46**, 5529 (2021).
- [57] M. Minder, M. Pittaluga, G. Roberts, M. Lucamarini, J. Dynes, Z. Yuan, and A. Shields, *Nat. Photonics* **13**, 334 (2019).
- [58] X. Zhong, J. Hu, M. Curty, L. Qian, and H.-K. Lo, *Phys. Rev. Lett.* **123**, 100506 (2019).
- [59] S. Wang, D.-Y. He, Z.-Q. Yin, F.-Y. Lu, C.-H. Cui, W. Chen, Z. Zhou, G.-C. Guo, and Z.-F. Han, *Phys. Rev. X* **9**, 021046 (2019).
- [60] Y. Liu, Z.-W. Yu, W. Zhang, J.-Y. Guan, J.-P. Chen, C. Zhang, X.-L. Hu, H. Li, C. Jiang, J. Lin, T.-Y. Chen, L. You, Z. Wang, X.-B. Wang, Q. Zhang, and J.-W. Pan, *Phys. Rev. Lett.* **123**, 100505 (2019).
- [61] X.-T. Fang, P. Zeng, H. Liu, M. Zou, W. Wu, Y.-L. Tang, Y.-J. Sheng, Y. Xiang, W. Zhang, H. Li, Z. Wang, L. You, M.-J. Li, H. Chen, Y.-A. Chen, Q. Zhang, C.-Z. Peng, X. Ma, T.-Y. Chen, and J.-W. Pan, *Nat. Photonics* **14**, 422 (2020).
- [62] J.-P. Chen, C. Zhang, Y. Liu, C. Jiang, W. Zhang, X.-L. Hu, J.-Y. Guan, Z.-W. Yu, H. Xu, J. Lin, M.-J. Li, H. Chen, H. Li, L. You, Z. Wang, X.-B. Wang, Q. Zhang, and J.-W. Pan, *Phys. Rev. Lett.* **124**, 070501 (2020).
- [63] H. Liu, C. Jiang, H.-T. Zhu, M. Zou, Z.-W. Yu, X.-L. Hu, H. Xu, S. Ma, Z. Han, J.-P. Chen, Y. Dai, S.-B. Tang, W. Zhang, H. Li, L. You, Z. Wang, Y. Hua, H. Hu, H. Zhang, F. Zhou, Q. Zhang, X.-B. Wang, T.-Y. Chen, and J.-W. Pan, *Phys. Rev. Lett.* **126**, 250502 (2021).
- [64] X. Zhong, W. Wang, L. Qian, and H.-K. Lo, *npj Quantum Inf.* **7**, 8 (2021).
- [65] J.-P. Chen, C. Zhang, C. Liu, Yang Jiang, W.-J. Zhang, Z.-Y. Han, S.-Z. Ma, X.-L. Hu, Y.-H. Li, F. Liu, Hui Zhou, H.-F. Jiang, H. Chen, Teng-Yun Li, L.-X. You, Z. Wang, X.-B. Wang, Q. Zhang, and J.-W. Pan, *Nat. Photonics* **15**, 570 (2021).
- [66] C. Clivati, A. Meda, S. Donadello, S. Virzi, M. Genovese, F. Levi, A. Mura, M. Pittaluga, Z. Yuan, A. J. Shields, M. Lucamarini, I. P. Degiovanni, and D. Calonico, *Nat. Commun.* **13**, 157 (2022).
- [67] M. Pittaluga, M. Minder, M. Lucamarini, M. Sanzaro, R. I. Woodward, M.-J. Li, Z. Yuan, and A. J. Shields, *Nat. Photonics* **15**, 530 (2021).
- [68] S. Wang, Z.-Q. Yin, D.-Y. He, W. Chen, R.-Q. Wang, P. Ye, Y. Zhou, G.-J. Fan-Yuan, F.-X. Wang, W. Chen, Y.-G. Zhu, P. V. Morozov, A. V. Divochiy, Z. Zhou, G.-C. Guo, and Z.-F. Han, *Nat. Photonics* **16**, 154 (2022).
- [69] W. Li, L. Zhang, Y. Lu, Z.-P. Li, C. Jiang, Y. Liu, J. Huang, H. Li, Z. Wang, X.-B. Wang, *et al.*, *arXiv preprint arXiv:2212.04311* (2022).
- [70] L. Zhou, J. Lin, Y. Jing, and Z. Yuan, *Nat. Commun.* **14**, 928 (2023).
- [71] Y.-M. Xie, B.-H. Li, Y.-S. Lu, X.-Y. Cao, W.-B. Liu, H.-L. Yin, and Z.-B. Chen, *Opt. Lett.* **46**, 1632 (2021).
- [72] Y.-M. Xie, Y.-S. Lu, C.-X. Weng, X.-Y. Cao, Z.-Y. Jia, Y. Bao, Y. Wang, Y. Fu, H.-L. Yin, and Z.-B. Chen, *PRX Quantum* **3**, 020315 (2022).
- [73] P. Zeng, H. Zhou, W. Wu, and X. Ma, *Nat. Commun.* **13**, 3903 (2022).
- [74] H.-T. Zhu, Y. Huang, H. Liu, P. Zeng, M. Zou, Y. Dai, S. Tang, H. Li, L. You, Z. Wang, *et al.*, *Phys. Rev. Lett.* **130**, 030801 (2023).
- [75] L. Zhou, J. Lin, Y.-M. Xie, Y.-S. Lu, Y. Jing, H.-L. Yin, and Z. Yuan, *arXiv preprint arXiv:2212.14190* (2022).
- [76] C. Jiang, Z.-W. Yu, X.-L. Hu, and X.-B. Wang, *Phys. Rev. A* **103**, 012402 (2021).
- [77] W.-Y. Hwang, *Phys. Rev. Lett.* **91**, 057901 (2003).
- [78] X.-B. Wang, *Phys. Rev. Lett.* **94**, 230503 (2005).
- [79] H.-K. Lo, X. Ma, and K. Chen, *Phys. Rev. Lett.* **94**, 230504 (2005).
- [80] X. Ma and M. Razavi, *Phys. Rev. A* **86**, 062319 (2012).
- [81] H.-L. Yin, M.-G. Zhou, J. Gu, Y.-M. Xie, Y.-S. Lu, and Z.-B. Chen, *Sci. Rep.* **10**, 14312 (2020).
- [82] C. Jiang, X.-L. Hu, H. Xu, Z.-W. Yu, and X.-B. Wang, *New J. Phys.* **22**, 053048 (2020).

- [83] P. Zeng, W. Wu, and X. Ma, Phys. Rev. Applied **13**, 064013 (2020).
- [84] Y.-M. Xie, Comparison of secret key rates, https://github.com/yuan-meixie/key_rate_comparison.
- [85] Y. Fu, H.-L. Yin, T.-Y. Chen, and Z.-B. Chen, Phys. Rev. Lett. **114**, 090501 (2015).
- [86] H.-L. Yin, Y. Fu, C.-L. Li, C.-X. Weng, B.-H. Li, J. Gu, Y.-S. Lu, S. Huang, and Z.-B. Chen, National Science Review nwac228 (2022).
- [87] C. C. W. Lim, M. Curty, N. Walenta, F. Xu, and H. Zbinden, Phys. Rev. A **89**, 022307 (2014).